The Cryosphere
Discussions
EGU
Open Access

Multi-model based estimation of sea ice volume variations in the Baffin Bay

Chao Min[1], Qinghua Yang[1], Longjiang Mu[2], Frank Kauker[2,3], Robert Ricker[2]

[1]School of Atmospheric Sciences, Sun Yat-sen University, and Southern Marine Science and Engineering Guangdong Laboratory (Zhuhai), Zhuhai, 519082, China
[2]Alfred Wegener Institute, Helmholtz Centre for Polar and Marine Research, 27570 Bremerhaven, Germany
[3] Ocean Atmosphere Systems, 20249 Hamburg, Germany

Correspondence to: Qinghua Yang (yangqh25@mail.sysu.edu.cn)

Abstract. Sea ice in Baffin Bay plays an important role in the deep water formation in the Labrador Sea and contributes to the variation of the Atlantic meridional overturning circulation (AMOC) on larger scales. To quantify the sea ice volume variations in Baffin Bay, a major driver of the deep water formation, three state-of-the-art sea ice models (CMST, NAOSIM, and PIOMAS) are investigated in the melt and freezing season from 2011 to 2016. An ensemble of three estimates of the sea ice volume fluxes in Baffin Bay is generated from the three modeled sea ice thickness and NSIDC satellite derived ice drift data. Results show that the net increase of the ensemble mean sea ice volume (SIV) in Baffin Bay occurs from October to April with the largest SIV increase in December (116 ± 16 km^3 month^{-1}) and the reduction occurs from May to September with the largest SIV decline in July (-160 ± 32 km^3 month^{-1}). The maximum SIV inflow occurs in winter in all the model data consistently. The ensemble mean SIV inflow (322 ± 4 km^3) reaches its maximum in winter 2013 caused by high ice velocities while the largest SIV outflow (244 ± 61 km^3) occurs in spring of 2014. The long-term annual mean ice volume inflow and outflow are $437(\pm53)$ km^3 and $339(\pm68)$ km^3, respectively. Our analysis also reveals that on average, sea ice in Baffin Bay melts from May to October with a net reduction of 335 km^3 in volume while it freezes from November to April with a net increase of 251 km^3.

1 Introduction

Baffin Bay is a semi-enclosed basin between Ellesmere Island, Baffin Island and Greenland. This bay serves as an important pathway of freshwater draining off from the Arctic into the North Atlantic Oceans (Curry et al., 2010; Curry et al., 2014). Locally, sea ice in Baffin Bay has a significant influence on Greenland coastal air temperatures and ice sheet surface-melt (Ballinger et al., 2018; Rennermalm et al., 2009; Stroeve et al., 2017). The sea ice condition in Baffin Bay also supports wildlife habitations (Ferguson et al., 2000; Laidre and Heide-Jørgensen, 2004; Spencer et al., 2014). Furthermore, marine-based activities, such as shipping, are strongly influenced by the sea ice conditions in the bay (Pizzolato et al., 2016). Therefore, understanding the sea ice variations in the Baffin Bay is of strong interest for climate change research but also for stakeholders. Landy et al. (2017) investigated the sea ice thickness (SIT) distribution and sea ice growth rate using satellite-based observations (e.g., SMOS, ICESat and CryoSat-2 SIT). However, seasonal thin sea ice in the bay is dominating and satellite-based ice thickness has large errors in the bay. For example, SMOS SIT usually underestimates the ice thickness when the ice

is thicker than 1.0 m and CryoSat-2 SIT has large uncertainties for thin ice below 1.0 m (Ricker et al., 2014; Tian-Kunze et al., 2014; Tietsche et al., 2018). In a recent study, Bi et al. (2019) analysed the sea ice area fluxes in the Baffin Bay on a long-term time period for the first time and the increasing trend of the annual sea ice area flux are found, i.e., 38.9×10^3 km^2 decade^{-1}

35   for the north gate, 82.2×10^3 km^2 decade^{-1} for south gate, and 7.5×10^3 km^2 decade^{-1} for Lancaster Sound, respectively. However, sea ice volume variations in Baffin Bay, strongly controlled by the sea ice volume inflow and outflow, are not investigated in that study. Cuny et al. (2005), Tang et al. (2004) and Kowk (2007) estimated the annual mean SIV outflow that export through Davis Strait into Baffin Bay based on a simple assumption of linear variation of mean SIT across the strait due to scarce SIT observations. They reported a mean SIV outflow through Davis Strait of about 528 km^3 year^{-1}, 873 km^3 year^{-1}

40   and 530-800 km^3 year^{-1}, respectively. Until several years ago, the mean SIV outflow (407 km^3 year^{-1}, from 2004 to 2010) averaged from November to May are approximately presented with the SIT observations rather than a simple SIT assumption from five upward looking sonars (ULSs) that moored in the Davis Strait (Curry et al., 2014). However, to the authors' knowledge, there is no such a study investigating the year-round SIV inflow and outflow covering the years of the lowest sea ice extent records (i.e., 2012 and 2016). Indeed, the freshwater budget is a function of sea ice formation and melting, input

45   from river water and land ice input (Landy et al., 2014; Landy et al., 2017). The sea ice thermodynamic processes are closely related to the desalination of seawater and the freshwater budget in the Baffin Bay.

In this study, we focus on the local sea ice volume variations in Baffin Bay. We define the SIV inflow and outflow gates located at ~73°N and ~68°N between Baffin Island and Greenland (Fig. 1), respectively, following Kwok (2007). Sea ice volume variations are calculated in the area between these two gates. There is limited *in-situ* observed SIT in this bay and also

50   the satellite-based SIT (i.e., SMOS, Crysat-2 and CS2SMOS) have large uncertainties and are inappropriate to be used directly in that area (Ricker et al., 2014; Ricker et al., 2017; Tian-Kunze et al., 2014; Tietsche et al., 2018). To address the challenging estimation of sea ice volume variations in Baffin Bay, three sea ice-ocean models driven by atmospheric reanalysis are employed, namely the sufficiently well validated CMST, the widely used PIOMAS and a version of NAOSIM with optimized parameters. CMST is based on the MITgcm ice-ocean model and sea ice thickness (SIT) and concentration (SIC) are

55   assimilated (Mu et al., 2018a) while PIOMAS assimilates SIC and sea surface temperature (SST) (Zhang and Rothrock, 2003; Schweiger et al., 2011). No sea ice data are assimilated in the NAOSIM simulation but the model parameters are optimized with a micro genetic algorithm (mGA) (Sumata et al., 2019a, b). Also, the recent TOPAZ4 reanalysis assimilates SIT in addition to other sea ice and ocean variables but only the time period 2014 to 2018 is covered (Xie et al., 2018), which is why it is only used to inter-compare with the other models in this study. Because very little *in-situ* observation can be used to

60   validate these SIT in Baffin Bay, we carry out an inter-comparison of SIT between CMST, NAOSIM, PIOMAS, TOPAZ4 and SMOS. Then, to obtain an estimate of the sea ice volume fluxes, we calculate the ensemble mean of the inflows and outflows from the three modeled sea ice thickness and the NSIDC ice drift, the only observed ice drift available the year round during the study period. Furthermore, since the Baffin Bay plays a crucial role as the primary source of freshwater and sea ice for the Labrador Sea (Curry et al., 2014; Tang et al., 2004), the amount of freshwater flux that exported into the Labrador Sea is

65   simply calculated based on the estimated outflow SIV fluxes exported through the Davis Strait.

This paper is organized as follows. Sea ice data sets and computing methods used in this study are described in section 2. In section 3, we present the major findings of this study. Discussions of SIIV flux uncertainties are given in section 4. In section 5, main findings are finally drawn.

2 Data and methods

2.1 CMST sea ice data

70   The complementarity of SMOS and CryoSat-2 SIT is utilized in CMST by assimilating SMOS SIT from University of Hamburg, CryoSat-2 SIT from AWI and Special Sensor Microwave Imager/Sounder (SSMIS) ice concentration into the MITgcm (Mu et al., 2018a). The ice-ocean model is forced by ensemble atmospheric forecasts from the UK Met Office (UKMO) taking the uncertainty of the atmospheric data into account (Yang et al., 2015). CMST provides daily sea ice thickness

75   (SIT), concentration (SIC) and drift (SID). CMST SIT is systematically validated within the Arctic basin by Mu et al. (2018a) and its SID were further validated against NSIDC and SAR data in the Fram Strait by Min et al. (2019). Additionally, CMST is applied successfully in Fram Strait and obtained a relatively accurate estimate of the year-round sea ice volume export through Fram Strait (Min et al., 2019).

2.3 NAOSIM sea ice data

80   The NAOSIM SIT data is produced by the regional sea ice-ocean model of the Arctic and northern North Atlantic Ocean (NAOSIM) developed at the Alfred Wegener Institute (Köberle and Gerdes, 2003; Kauker et al., 2003; Karcher et al., 2007). The model is forced by the NCEP Climate Forecast System version 2 (Saha et al. 2014). 15 model parameters (e.g., ice strength, drag coefficients) were optimized simultaneously using a micro genetic algorithm (mGA). A detailed description of NAOSIM and the methodology used for the optimization can be found in Sumata et al. (2019a, b). The model version used in this study

85   distinguishes from the model version applied for the optimization in Sumata et al. (2019a, b) by a horizontal resolution of about 28km (Model version MR in Sumata et al. (2019a)). The parameters (except the vertical mixing coefficient) are taken from the third optimization of Sumata et al. (2019b) termed OPT-3.

2.4 PIOMAS sea ice data

The widely used Pan-Arctic Ice-Ocean Modeling and Assimilation System (PIOMAS) SIT data is produced by a sea-ice ocean

90   model that assimilates near-real-time daily SIC from National Snow and Ice Data Center (NSIDC), atmospheric forcing and sea surface temperature from National Centers for Environmental Prediction (NCEP) and National Center for Atmospheric Research (NCAR) reanalysis by nudging and optimal interpolation (Zhang and Rothrock, 2003; Schweiger et al., 2011; Zhang and Rothrock, 2003). Effective sea ice thickness data are provided operationally from 1978 on and is permanently updated. In this study, we use the monthly SIT data of PIOMAS V2.1 from 2011 to 2016.

2.4 TOPAZ4 sea ice data

TOPAZ4 is an ocean and sea-ice prediction system. The ocean model is based on the Hybrid Coordinate Ocean Model (HYCOM version 2.2) (Bleck, 2002; Chassignet et al., 2003). The sea-ice model employs the one-thickness category and elastic-viscous-plastic rheology (Bouillon et al., 2013; Hunke and Dukowicz, 1997). The system is forced by ERA-interim atmospheric reanalysis. Ocean and sea ice observations are assimilated into TOPAZ4 (e.g., the along track sea level anomaly and gridded sea surface temperature, sea ice concentration, and CS2SMOS SIT) (Xie et al., 2018). Since the TOPAZ4 reanalysis data covers only the years 2014 to 2018, in this study, the TOPAZ4 SIT and SID are only used for inter-comparison with the other simulations.

2.5 SMOS sea ice data

The Soil Moisture and Ocean Salinity (SMOS) SIT data are retrieved from the Microwave Imaging Radiometer using Aperture Synthesis (MIRAS) measured brightness temperatures in the L-band (1.4 GHz) (Tian-Kunze et al., 2014). The SMOS SIT data (V3.1) are compared with the model data. The SMOS SIT is accurate when the ice is thinner than 50 cm, but its uncertainty becomes larger when the ice becomes thicker. The SMOS SIT observations are utilized because *in-situ* observed SIT data are very scarce in Baffin Bay, and the Crysat-2/CS2SMOS SIT data are inappropriate in this area with strong seasonality (Ricker et al., 2014; Ricker et al., 2017). We should keep in mind that the SMOS SIT data underestimate the SIT in the Baffin Bay mainly because the 100% ice concentration assumption during the data retrieval is not full filed (Tian-Kunze et al., 2014; Tietsche et al., 2018).

2.6 NSIDC SID data

The Polar Pathfinder Daily 25 km EASE-Grid sea ice drift data (V4) from NSIDC are used to calculate SIV fluxes because it contains year-round date for the time period investigated. The AVHRR, AMSR-E, SMMR, SSM/I, SSM/I, International Arctic Buoy Program (IABP) buoys observations and reanalysis wind data are integrated to derive the NSIDC sea ice motion (Tschudi et al., 2019; Tschudi et al., 2020). The NSIDC SID data are chosen as a reference to evaluate model ice drift and they are applied to calculate the sea ice flux, since they cover the time span from 2011 to 2016 including summer seasons. Moreover, the NSIDC data set has been recently validated in the Baffin Bay by Bi et al. (2019).

2.7 Retrieving methods in SIV flux

We use monthly mean sea ice thickness and drift to obtain the SIV fluxes following Meier et al. (2006) and Ricker et al. (2018). The formulas to derive the SIV inflows and outflows are same as applied in Min et al. (2019):

$$Q_{flux} = L \, H \, v, \tag{1}$$

The Cryosphere
Discussions
EGU Open Access

where Q_{flux} represent the SIV fluxes at the north and south gates. L and H are zonal interpolated grid width and corresponding SIT along the two gates, respectively. The meridional velocity v is also utilized to estimate the sea ice flux (inflows and

125 outflows). The SIC is not involved in equations (1), because they are already used to calculate the effective thickness in CMST, NAOSIM and PIOMAS. It is difficult to identify the most accurate SIT simulation and ice flux estimation, so we adopt the ensemble approach to estimate the sea ice variations in the Baffin Bay, i.e., ensemble mean inflows and outflows are from (1) CMST SIT and NSIDC SID, (2) NAOSIM SIT and NSIDC SID, (3) PIOMAS SIT and NSIDC SID (equation (1)). Analogously, the sea ice volume in the Baffin Bay is calculated from the ensemble mean of CMST, NAOSIM and PIOMAS.

130 Following Ricker et al. (2018) and Bi et al. (2019), the sea ice volume variation can be derived as follows:

$$\frac{dV}{dt} = Q_{net} + \left(\frac{dV_{therm}}{dt} + \frac{dV_{resid}}{dt} \right), \tag{2}$$

where dV/dt represents the monthly SIV change in the Baffin Bay. Q_{net} is the monthly net SIV flux (Δflux) estimated by the difference between inflow and outflow (i.e., ice inflow minus outflow). As suggested by Robert et al. (2018), quantifying thermodynamic growth (dVtherm/dt) and residual contributions (dVresid/dt), due to dynamics and deformation, is challenging.

135 Therefore, we only consider their integral contribution. Eventually, the integral contribution of dVtherm/dt and dVresid/dt is regarded as thermodynamic SIV growth rate in this study. To distinguish ice melting and freezing, we use negative thermodynamic SIV growth rates to represent reduction through ice melting and positive rates to denote growth due to freezing.

3 Results

The spatial distribution of the ensemble mean SIC, SIT and SID in March, July and October are shown in Fig. 1. We have

140 chosen these months as they are a typical representation for the seasonal cycle. Meier et al. (2006) reported that the maximum extent occurs in March while July is the last month when sea ice is still left, and the ice freeze-up starts in October. Furthermore, we present the spatial variation of SIT especially in July when satellite-based SIT is not available due to melting processes. The ensemble mean SIT shows that the thicker ice (>1.2 m) is located east of Baffin Island in March while largest ice velocities are found near the south gate in March. The spatial distribution of ensemble mean SIT in March is similar to that found in

145 Landy et al. (2017). Similarly, the sea ice that thicker than 0.3 m is located near the eastern coast of Baffin Island in the Baffin Bay in July. When focusing on the freeze-up period (October), we found the ice located near the Nares Strait is mostly thicker than 0.5 m, and higher ice velocity (more than 10 km day^{-1}) is also found near the Smith Sound and Lancaster Sound by CMST (figure not shown).

The comparison of SIT (averaged along the north and south gates) between CMST, NAOSIM, PIOMAS, TOPAZ4 and SMOS

150 is shown in Fig. 2a and 2b, respectively. The sea ice drift from CMST, NAOSIM, PIOMAS, TOPAZ4 and NSIDC are compared with each other as well (Fig. 2c and 2d). The SIC variation is not shown here because the models (except NAOSIM) have already taken SIC into account via the assimilation. In general, the sea ice properties show a significant annual cycle with the mean SIT thinner than 1 m for both the north and the south gates. Compared with the satellite-observed SMOS SIT, all of

these SIT simulations present thicker ice thickness than SMOS (Fig. 2a and 2b). Specifically, the mean SIT averaged along

155   the north gate is 0.72 m for CMST, 0.83 m for NAOSIM, 0.84 m for PIOMAS and 0.55 m for TOPAZ4 during the freezing

season while the mean SIT is only 0.47 m for SMOS. Likewise, the mean SIT averaged along the south gate is only 0.31 m

for SMOS while the mean SITs of CMST, NAOSIM, PIOMAS and TOPAZ4 are 0.52 m, 0.61 m 0.72 m and 0.44 m,

respectively. In addition, the SIT simulations from NAOSIM and PIOMAS show a thicker estimation of sea ice than the CMST

and TOPAZ4 data that assimilate satellite-observed SIT, while the SIT trends of CMST and TOPAZ4 are more consistent with

160   SMOS. Furthermore, sea ice drift (SID) contributes much more to sea ice flux variation on its monthly scale (Min et al., 2019;

Ricker et al., 2018). For this reason, an accurate simulation of SID is another vital factor to derive sea ice volume flux. Again,

because of the all-year round coverage and the recent validation of NSIDC drift in the Baffin Bay by Bi et al. (2019), we apply

NSIDC drift to calculate the sea ice flux in this study. In addition, we conduct an inter-comparison of SID between NSIDC,

CMST, NAOSIM, PIOMAS and TOPAZ4 in Fig. 2c and 2d to examine the performance of these modeled SID data. Note that

165   the TOPAZ4 values are from 2014-2016 for the overlapped period. A fairly similar trend of SID is shown by CMST, TOPAZ4

and NSIDC but both CMST and TOPAZ4 present a higher ice velocity than that from NSIDC while NAOSIM and PIOMAS

underestimate the monthly mean ice drift. Moreover, TOPAZ4 simulates the fastest ice velocity among five data sets while

PIOMAS shows the lowest ice drift across the north gate. We calculate the correlation coefficients (CCs) between these model

simulations and the reference NSIDC ice drift. The highest significant ($\alpha=0.05$) CCs (0.94 and 0.92) are found between

170   TOPAZ4 and NSIDC SID while it overestimates the ice drift compared to NSIDC by around 52% and 82% along the north

gate and south gates, respectively. CMST shows also high CCs compared with NSIDC drift in both two gates, the correlations

are 0.90 (significant) along the north gate and 0.91 (significant) along the south gate with an overestimation of 40% and 70%,

respectively. The ice drift produced by NAOSIM and PIOMAS show relatively low CCs against NSIDC drift. As an example,

the CCs between NAOSIM and NSIDC drift are 0.61 (non-significant) and 0.61 (non-significant) along the north and south

175   gates, respectively. The coefficients between PIOMAS and NSIDC drift are also relatively low as it is only 0.60 (significant)

for the north gate and 0.71 (non-significant) for the south gate, respectively.

Although CMST and NSIDC drift correlate very well over the time span from 2011 to 2016, modeled SID shows a large

overestimation of the drift. Therefore, we conclude that modeled SID is with large uncertainties and we calculate ice flux

estimations from CMST, NAOSIM, PIOMAS thickness and NSIDC drift, i.e. without the usage of any modeled ice drift.

180   The sea ice imported into the Baffin Bay through the north gate can be divided into three sources: Sea ice input (including

multi-year ice) from Nares Strait, Lancaster Sound and Jones Sound that originate from the Arctic Ocean and the Canadian

Arctic Archipelago (CAA); and moreover, a large amount of ice is generated in recurring polynyas, i.e., the North Water

(NOW) Polynya (Bi et al, 2019; Kwok, 2007, 2005). In our study, we only focus on the total amount of ice inflow through the

north gate, so the ice from the Arctic Ocean, the CAA and the NOW Polynya are summed up to derive the sea ice inflow

185   through the north gate.

Considering that the further developed CryoSat-2 and SMOS SIT data are successfully utilized to calculate the sea ice volume

variation in the Baffin Bay (Landy et al., 2017), CMST which assimilates both CryoSat-2 and SMOS SIT and SSMIS ice

concentration is together applied with the widely used PIOMAS and the parameter-optimized NAOSIM to estimate the SIV

inflows, outflows and thermodynamic SIV growth from 2011 to 2016. The monthly and seasonal mean ice inflows and

190   outflows from 2011 to 2016 are shown in Fig. 3 and 4, respectively. The sea ice volume (SIV) flux calculated by the four data

sets (mentioned in methodology section 2.7) shows a good consistency between 2011 and 2016 (Fig. 3). In total, the ensemble

mean SIV inflow and outflow are $437(\pm53)$ km^3 and $339(\pm68)$ km^3 per year, respectively. Even though there are some

disparities between these three fluxes calculated from the different models (CMST, NAOSIM and PIOMAS), these fluxes

show a consistent trend of seasonal variation (in term of the ensemble standard deviation). In general, the maximum ice inflows

195   occur in February and March (89 ± 4 km^3 month^{-1} and 89 ± 12 km^3 month^{-1}, respectively). Here, we define spring as the time span

from March to May, summer from June to August, autumn from September to November, and winter from December to

February, respectively. Seasonal sea ice inflows and outflows from the three models show better consistency in the inflows

than outflows, which we attribute to the larger discrepancies of the ice thickness along the south gate between CMST, PIOMAS

and NAOSIM. In average the maximum of ice inflows occur in winter with a mean value of $251(\pm12)$ km^3 while ice outflows

200   usually reach the maximum in spring/winter with a mean value of $217 (\pm44)$ km^3. The maximum of SIV inflow (322 ± 4 km^3)

occurs in winter 2013 because of the largest sea ice drift even if the ice thickness is not at its maximum. The SIV inflow in the

melt season (May-September) is only 8% of that in the freezing season (October–April) and the SIV outflow in the melt season

only accounts for 10% of that in the freezing season. Furthermore, to quantify the fresh water imported into the Labrador Sea,

where it is an important area of deep water formation, we convert the sea ice volume outflows to the fresh water fluxes by

205   multiplying a factor of 0.8 following Spreen et al. (2020). The monthly mean fresh water fluxes are shown in Table 1. Annually,

the amount of freshwater flux that exported into the Labrador Sea derived from sea ice volume flux is bout 271 km^3 year $^{-1}$.

Relatively large fresh water fluxes are found from January to April peaking at 71 km^3 month^{-1} in March.

It is essential to quantify the sea ice volume variations in the Baffin Bay because the desalination of seawater and the freshwater

budget are affected by the sea ice thermodynamic processes (Landy et al., 2014; Landy et al., 2017). The locally

210   thermodynamic processes are further invested considering sea ice freezing and melting (Fig. 5). The ensemble mean SIV in

the Baffin Bay increases from October to April with a maximum rate of 116 ± 16 km^3 month^{-1} in December. It decreases from

May to September with a maximum reduction rate of -160 ± 32 km^3 month^{-1} in July. Consistently, the net ice volume flux

exported into the Baffin Bay occurs from October to January with a maximum of 47 ± 8 km^3 month^{-1} in December. Moreover,

we analyze the thermodynamic SIV growth rate that is divided into net ice freezing and melting growth in Fig. 5b. In average,

215   we find that the ice freezes from November to April with a mean ice freezing rate of 36 km^3 month^{-1} while the maximum

freezing rate occurs in December (70 km^3 month^{-1}). The ice melting occurs from May to October with a monthly mean of -67

km^3 month^{-1} while the maximum occurs in July (-160 km^3 month^{-1}). Taking these thermodynamic SIV growth into account,

we could infer that the surface seawater salinity increases from November to April and decreases from May to October because

of the close connection between sea ice formation/melting and the freshwater budget.

4 Discussions

The sea ice imported into the Baffin Bay is mainly from Nares Strait, Lancaster Sound, Jones Sound, and recurring polynyas, i.e., the North Water (NOW) Polynya (Bi et al, 2019; Kwok, 2007, 2005). Kwok (2007 and 2005) pointed out that the SIV export from the Arctic through the Robeson Channel becomes most active after July. And we notice that the ice thicker than 0.5 m is mostly located near the Nares Strait companying with higher ice velocity (more than 10 km day^{-1}) found near the Smith Sound and Lancaster Sound by CMST (figure not shown). We thus speculate that the thick ice is exported from the Arctic since the higher ice velocity is also found in these areas, and the faster ice is usually deemed to be a proxy for higher ice flux. This is also noticed in previous studies (Kwok, 2007, 2005).

Sea ice freezing and melting processes in Baffin Bay and SIV fluxes exported through the Davis Strait are significant for the deep water formation in the Labrador Sea. Landy et al. (2017) investigated the sea ice variation rate within the scope of the variability in total ice volume neglecting detailed contributions of ice influx, outflux and formation/melting evolutions. In this study, we further estimate the thermodynamic processes considering sea ice freezing and melting in the Baffin Bay. We noticed that it is different from the sea ice extent evolution reported by Meier et al. (2006) who found a maximum in March while we find a maximum of the SIV in April.

It should be noted that, because of the very limited *in-situ* SIT observations in the Baffin Bay, it is not possible to identify very accurate sea ice flux in this area. But a series of detailed validations of CMST, PIOMAS, TOPAZ4 and NAOSIM SIT are already performed in the Arctic basin and the Fram Strait (Min et al., 2019; Mu et al., 2018a; Wang et al., 2016; Xie et al., 2018, Sumata et al., 2019a and b). The aim of this study is to give a state-of-the-art ensemble mean estimation of SIV flux based on a combination of model results and observations, and to conduct a first estimate of the thermodynamic growth of sea ice volume. Additionally, this is the first study using the three totally different sea ice data model data that assimilate both SIC and SIT (CMST), without any SIT assimilation (PIOMAS), and without any assimilation but optimized model parameters (NAOSIM) to estimate an ensemble mean sea ice variations in the Baffin Bay. To the authors' knowledge, we potentially underestimate the ice fluxes in the Baffin Bay with of the usage of NSIDC drift, so long-term sea ice drift data in the bay still need to be further developed. We also notice that there are some discrepancies among CMST, PIOMAS and NAOSIM thickness. For instance, the sea ice reduction period of NAOSIM and PIOMAS start later than that of CMST in Baffin Bay (Fig 6). CMST SIT shows a much more coherent ice thickness to the satellite observations, e.g., the sea ice volume variation shown by CMST reaches its maximum in March (Fig. 6) which is also found by Landy et al. (2017). However, the monthly mean variability shows a consistent start (October) of ice volume growth. Moreover, all of these simulations reach their maximum SIV increase and decline in December and July, respectively. Compared to the model data without SIT assimilation (NAOSIM and PIOMAS), CMST and TOPAZ4 have more similar variability to SMOS (shown in Fig. 1a and 1b). However, it is impossible to identify the sea ice simulation which is most accurate in this area without *in-situ* observations. We thus applied an ensemble approach to give a state-of-the-art estimation of sea ice flux, volume and the thermodynamic SIV growth in the Baffin Bay. Consequently, we strongly suggest that the international communities of marine/polar science should work

The Cryosphere
Discussions

Open Access

EGU

together to carry out more long-term sea ice observations in Baffin Bay to allow for better validation of satellite -based sea ice data and model simulations.

5 Conclusions

In order to examine the sea ice volume variations in Baffin Bay, we calculated the ensemble mean SIV flux and thermodynamic SIV growth from multi-model thickness data and NSIDC ice drift. Main conclusions can be summarized as follows:

(1) The sea ice volume (SIV) reaches its maximum in April. It starts to increase from October until the melt season while the reduction occurs from May to September. The averaged maximum growth rate of 116 ± 16 km^3 month^{-1} is found in December, while the maximum reduction rate of -160 ± 32 km^3 month^{-1} is in July.

(2) The annual mean SIV inflow and outflow are $437(\pm53)$ km^3 year^{-1} and $339(\pm68)$ km^3 year^{-1}, respectively. The SIV inflow in the melt season is only 8% of that in the freezing season. The SIV outflow in the melt season is a small fraction (10%) of the outflow in the freezing season. The maxima of ice inflows occur in winter.

(3) The maximum SIV freezing growth rate (70 km^3 month^{-1}) occurs in December while the maximum melting reduction rate (-160 km^3 month^{-1}) happens in July. In average, ice freezing (251 km^3) takes place from November to April while the ice melting (-355 km^3) occurs from May to October indicating that the surface seawater salinity may increase from November to April and decrease from May to October, correspondingly.

(4) The freshwater flux that imported into the Labrador Sea derived from sea ice volume flux is bout 271 km^3 year^{-1} and is mainly from December to May. The peaking rate of freshwater flux is about 71 km^3 month^{-1} in March. We thus infer that the surface seawater will be desalinated as a result from sea ice melting in the Labrador Sea from December to May.

Author contributions. CM and QY conceptualized this study. CM carried out these estimations and wrote the paper. FF provided the NAOSIM sea ice data. All co-authors assisted during the writing process and improved the readability of this paper.

The Cryosphere
Discussions
Open Access
EGU

References

Ballinger, T. J., Hanna, E., Hall, R. J., Miller, J., Ribergaard, M. H., and Høyer, J. L.: Greenland coastal air temperatures linked to Baffin Bay and Greenland Sea ice conditions during autumn through regional blocking patterns, Clim. Dyn., 50, 83-100,
290 doi: 10.1016/j.dsr.2004.10.006, 2018.

Bi, H., Zhang, Z., Wang, Y., Xu, X., Liang, Y., Huang, J., Liu, Y., and Fu, M.: Baffin Bay sea ice inflow and outflow: 1978–1979 to 2016–2017, The Cryosphere, 13, 1025-1042, doi: 10.5194/tc-13-1025-2019, 2019.

Bleck, R.: An oceanic general circulation model framed in hybrid isopycnic-Cartesian coordinates, Ocean Model., 4, 55-88, doi: 10.1016/S1463-5003(01)00012-9, 2002.

295 Bouillon, S., Fichefet, T., Legat, V., and Madec, G.: The elastic-viscous-plastic method revisited, Ocean Model., 71, 2-12, doi: 10.1016/j.ocemod.2013.05.013, 2013.

Chassignet, E. P., Smith, L. T., Halliwell, G. R., and Bleck, R.: North Atlantic Simulations with the Hybrid Coordinate Ocean Model (HYCOM): Impact of the Vertical Coordinate Choice, Reference Pressure, and Thermobaricity, J. Phys. Oceanogr., 33, 2504-2526, doi: 10.1175/1520-0485(2003)033<2504:NASWTH>2.0.CO;2, 2003.

300 Cuny, J., Rhines, P. B., and Kwok, R.: Davis Strait volume, freshwater and heat fluxes, Deep Sea Res. P. I., 52, 519-542, doi: 10.1016/j.dsr.2004.10.006, 2005.

Curry, B., Lee, C. M., and Petrie, B.: Volume, Freshwater, and Heat Fluxes through Davis Strait, 2004–05, J. Phys. Oceanogr., 41, 429-436, doi: 10.1175/2010JPO4536.1, 2010.

Curry, B., Lee, C. M., Petrie, B., Moritz, R. E., and Kwok, R.: Multiyear Volume, Liquid Freshwater, and Sea Ice Transports
305 through Davis Strait, 2004–10, J. Phys. Oceanogr., 44, 1244-1266, doi: 10.1175/JPO-D-13-0177.1, 2014.

Ferguson, S. H., Taylor, M. K., and Messier, F.: Influence of sea ice dynamics on habitat selection by polar bears, Ecology, 81, 761-772, doi: 10.2307/177375, 2000.

Hibler, W. D.: A Dynamic Thermodynamic Sea Ice Model, J. Phys. Oceanogr., 9, 815-846, doi: 10.1175/1520-0485(1979)009<0815:ADTSIM>2.0.CO;2, 1979.

310 Hunke, E. C. and Dukowicz, J. K.: An Elastic–Viscous–Plastic Model for Sea Ice Dynamics, J. Phys. Oceanogr., 27, 1849-1867, doi: 10.1175/1520-0485(1997)027<1849:AEVPMF>2.0.CO;2, 1997.

Karcher, M., Kauker, F., Gerdes, R., Hunke, E., and Zhang, J.: On the dynamics of Atlantic Water circulation in the Arctic Ocean, J. Geophys. Res-Oceans., 112, C04S02, doi:10.1029/2006JC003630, 2007.

Kauker, F., Gerdes, R., Karcher, M., and Köberle, C.: Impact of North Atlantic Current changes on the Nordic Seas and the Arctic Ocean, J. Geophys. Res-Oceans., 110, C12002, doi:10.1029/2004JC002624, 2005.

Kauker, F., Gerdes, R., Karcher, M., Köberle, C., and Lieser, J. L.: Variability of Arctic and North Atlantic sea ice: A combined analysis of model results and observations from 1978 to 2001, J. Geophys. Res-Oceans., 108, 3182, doi:10.1029/2002JC001573, 2003.

Köberle, C., and Gerdes, R.: Mechanisms Determining the Variability of Arctic Sea Ice Conditions and Export. J. Climate, 16, 2843–2858, doi: 10.1175/1520-0442(2003)016<2843:MDTVOA>2.0.CO;2. 2003.

Kwok, R.: Baffin Bay ice drift and export: 2002–2007, Geophys. Res. Lett., 34, L19501, doi:10.1029/2007GL031204, 2007.

Kwok, R.: Variability of Nares Strait ice flux, Geophys. Res. Lett., 32, L24502, doi:10.1029/2005GL024768, 2005.

Laidre, K. L. and Heide-Jørgensen, M. P.: Arctic sea ice trends and narwhal vulnerability, Biol. Conserv., 121, 509-517, doi: 10.1016/j.biocon.2004.06.003, 2004.

Landy, J., Ehn, J., Shields, M., and Barber, D.: Surface and melt pond evolution on landfast first-year sea ice in the Canadian Arctic Archipelago, J. Geophys. Res-Oceans., 119, 3054-3075, doi: doi:10.1002/2013JC009617, 2014.

Landy, J. C., Ehn, J. K., Babb, D. G., Thériault, N., and Barber, D. G.: Sea ice thickness in the Eastern Canadian Arctic: Hudson Bay Complex & Baffin Bay, Remote Sens. Environ., 200, 281-294, doi: 10.1016/j.rse.2017.08.019, 2017.

Meier, W. N., Stroeve, J., and Gearheard, S.: Bridging perspectives from remote Sensing and Inuit communities on changing Sea-ice cover in the Baffin Bay region, Ann. Glaciol., 44, 433-438, doi: 10.3189/172756406781811790, 2006.

Min, C., Mu, L., Yang, Q., Ricker, R., Shi, Q., Han, B., Wu, R., and Liu, J.: Sea ice export through the Fram Strait derived from a combined model and satellite data set, The Cryosphere, 13, 3209-3224, doi: 10.5194/tc-13-3209-2019, 2019.

Mu, L., Losch, M., Yang, Q., Ricker, R., Losa, S., and Nerger, L.: The Arctic sea ice drift simulation from October 2010 to December 2016, doi: 10.1594/PANGAEA.906973, 2019.

Mu, L., Losch, M., Yang, Q., Ricker, R., Losa, S. N., and Nerger, L.: Arctic-Wide Sea Ice Thickness Estimates From Combining Satellite Remote Sensing Data and a Dynamic Ice-Ocean Model with Data Assimilation During the CryoSat-2 Period, J. Geophys. Res-Oceans., 123, 7763-7780, doi: 10.1029/2018JC014316, 2018a.

Mu, L., Losch, M., Yang, Q., Ricker, R., Losa, S., and Nerger, L.: The Arctic combined model and satellite sea ice thickness (CMST) dataset, doi: 10.1594/PANGAEA.891475, 2018b.

Pizzolato, L., Howell, S. E. L., Dawson, J., Laliberté, F., and Copland, L.: The influence of declining sea ice on shipping activity in the Canadian Arctic, Geophys. Res. Lett., 43, 12,146–12,154, doi:10.1002/2016GL071489, 2016.

Rennermalm, A. K., Smith, L. C., Stroeve, J. C., and Chu, V. W.: Does sea ice influence Greenland ice sheet surface-melt?, Environmental Research Letters, 4, 024011, doi: 10.1088/1748-9326/4/2/024011, 2009.

Ricker, R., Girard-Ardhuin, F., Krumpen, T., and Lique, C.: Satellite-derived sea ice export and its impact on Arctic ice mass balance, The Cryosphere, 12, 3017-3032, doi: 10.5194/tc-12-3017-2018, 2018.

Ricker, R., Hendricks, S., Helm, V., Skourup, H., and Davidson, M.: Sensitivity of CryoSat-2 Arctic sea-ice freeboard and thickness on radar-waveform interpretation, The Cryosphere, 8, 1607-1622, doi: doi:10.5194/tc-8-1607-2014, 2014.

Ricker, R., Hendricks, S., Kaleschke, L., Tian-Kunze, X., King, J., and Haas, C.: A weekly Arctic sea-ice thickness data record from merged CryoSat-2 and SMOS satellite data, The Cryosphere, 11, 1607-1623, doi: 10.5194/tc-11-1607-2017, 2017.

350   Schweiger, A., Lindsay, R., Zhang, J., Steele, M., Stern, H., and Kwok, R.: Uncertainty in modeled Arctic sea ice volume, J. Geophys. Res-Oceans., 116, C00D06, doi:10.1029/2011JC007084, 2011.

Saha, S., Moorthi, S., Wu, X., Wang, J., Nadiga, S., Tripp, P., Behringer, D., Hou, Y.-T., Chuang, H.-y., Iredell, M., Ek, M., Meng, J., Yang, R., Mendez, M. P., van den Dool, H., Zhang, Q., Wang, W., Chen, M., and Becker, E.: The NCEP Climate Forecast System Version 2, J. Climate, 27, 2185–2208, doi: 10.1175/JCLI-D-12-00823.1, 2014.

355   Semtner, A. J.: A Model for the Thermodynamic Growth of Sea Ice in Numerical Investigations of Climate, J. Phys. Oceanogr., 6, 379-389, doi: 10.1175/1520-0485(1976)006<0379:AMFTTG>2.0.CO;2, 1976.

Spencer, N. C., Grant, G. H., L., M. M., and Hans-Ulrich, P.: Annual Movement Patterns of Endangered Ivory Gulls: The Importance of Sea Ice, Plos One, 9, e115231, doi: 10.1371/journal.pone.0115231, 2014.

Spreen, G., de Steur, L., Divine, D., Gerland, S., Hansen, E., & Kwok, R.: Arctic sea ice volume export through Fram Strait
360   from 1992 to 2014, J. Geophys. Res-Oceans., 125, e2019JC016039, doi: 10.1029/2019JC016039, 2020.

Stroeve, J. C., Mioduszewski, J. R., Rennermalm, A., Boisvert, L. N., Tedesco, M., and Robinson, D.: Investigating the local-scale influence of sea ice on Greenland surface melt, The Cryosphere, 11, 2363-2381, doi: 10.5194/tc-11-2363-2017, 2017.

Sumata, H., Kauker, F., Karcher, M., and Gerdes, R.: Covariance of Optimal Parameters of an Arctic Sea Ice–Ocean Model, Mon. Wea. Rev., 147, 2579-2602, doi: 10.1175/MWR-D-18-0375.1, 2019a.

365   Sumata, H., Kauker, F., Karcher, M., and Gerdes, R.: Simultaneous Parameter Optimization of an Arctic Sea Ice–Ocean Model by a Genetic Algorithm, Mon. Wea. Rev., 147, 1899-1926, doi: 10.1175/MWR-D-18-0360.1, 2019b.

Tang, C. C. L., Ross, C. K., Yao, T., Petrie, B., DeTracey, B. M., and Dunlap, E.: The circulation, water masses and sea-ice of Baffin Bay, Prog. Oceanogr., 63, 183-228, doi: 10.1016/j.pocean.2004.09.005, 2004.

Tian-Kunze, X., Kaleschke, L., Maaß, N., Mäkynen, M., Serra, N., Drusch, M., and Krumpen, T.: SMOS-derived thin sea ice
370   thickness: algorithm baseline, product specifications and initial verification, The Cryosphere, 8, 997-1018, doi: 10.5194/tc-8-997-2014, 2014.

Tietsche, S., Alonso-Balmaseda, M., Rosnay, P., Zuo, H., Tian-Kunze, X., and Kaleschke, L.: Thin Arctic sea ice in L-band observations and an ocean reanalysis, The Cryosphere, 12, 2051-2072, doi: 10.5194/tc-12-2051-2018, 2018.

Tschudi, M.A., W.N. Meier, and J.S. Stewart, 2020. An enhancement to sea ice motion and age products at the National Snow
375   and Ice Data Center (NSIDC). The Cryosphere, 14,1519-1536, doi: 10.5194/tc-14-1519-2020.

Tschudi, M., Meier, W. N., Stewart, J. S., Fowler, C., and Maslanik, J.: Polar Pathfinder Daily 25km EASE-Grid Sea Ice Motion Vectors, Version 4, Boulder, Colorado USA, NASA National Snow and Ice Data Center Distributed Active Archive Center, doi: 10.5067/INAWUWO7QH7B, 2019.

Wang, X., Key, J., Kwok, R., and Zhang, J.: Comparison of Arctic Sea Ice Thickness from Satellites, Aircraft, and PIOMAS
380   Data, Remote Sens., 8, 713, doi: 10.3390/rs8090713, 2016.

Warren, S. G., Rigor, I. G., Untersteiner, N., Radionov, V. F., Bryazgin, N. N., Aleksandrov, Y. I., and Colony, R.: Snow
Depth on Arctic Sea Ice, J. Climate, 12, 1814-1829, doi: 10.1175/1520-0442(1999)012<1814:SDOASI>2.0.CO;2, 1999.

Xie, J., Counillon, F., and Bertino, L.: Impact of assimilating a merged sea-ice thickness from CryoSat-2 and SMOS in the
Arctic reanalysis, The Cryosphere, 12, 3671-3691, doi: 10.5194/tc-12-3671-2018, 2018.

385   Yang, Q., Losa, S. N., Losch, M., Jung, T., and Nerger, L.: The role of atmospheric uncertainty in Arctic summer sea ice data
assimilation and prediction, Q.J.R. Meteorol. Soc., 141, 2314-2323, doi: 10.1002/qj.2523, 2015.

Zhang, J. and Rothrock, D. A.: Modeling Global Sea Ice with a Thickness and Enthalpy Distribution Model in Generalized
Curvilinear Coordinates, Mon. Wea. Rev., 131, 845-861, doi: 10.1175/1520-0493(2003)131<0845:MGSIWA>2.0.CO;2, 2003.
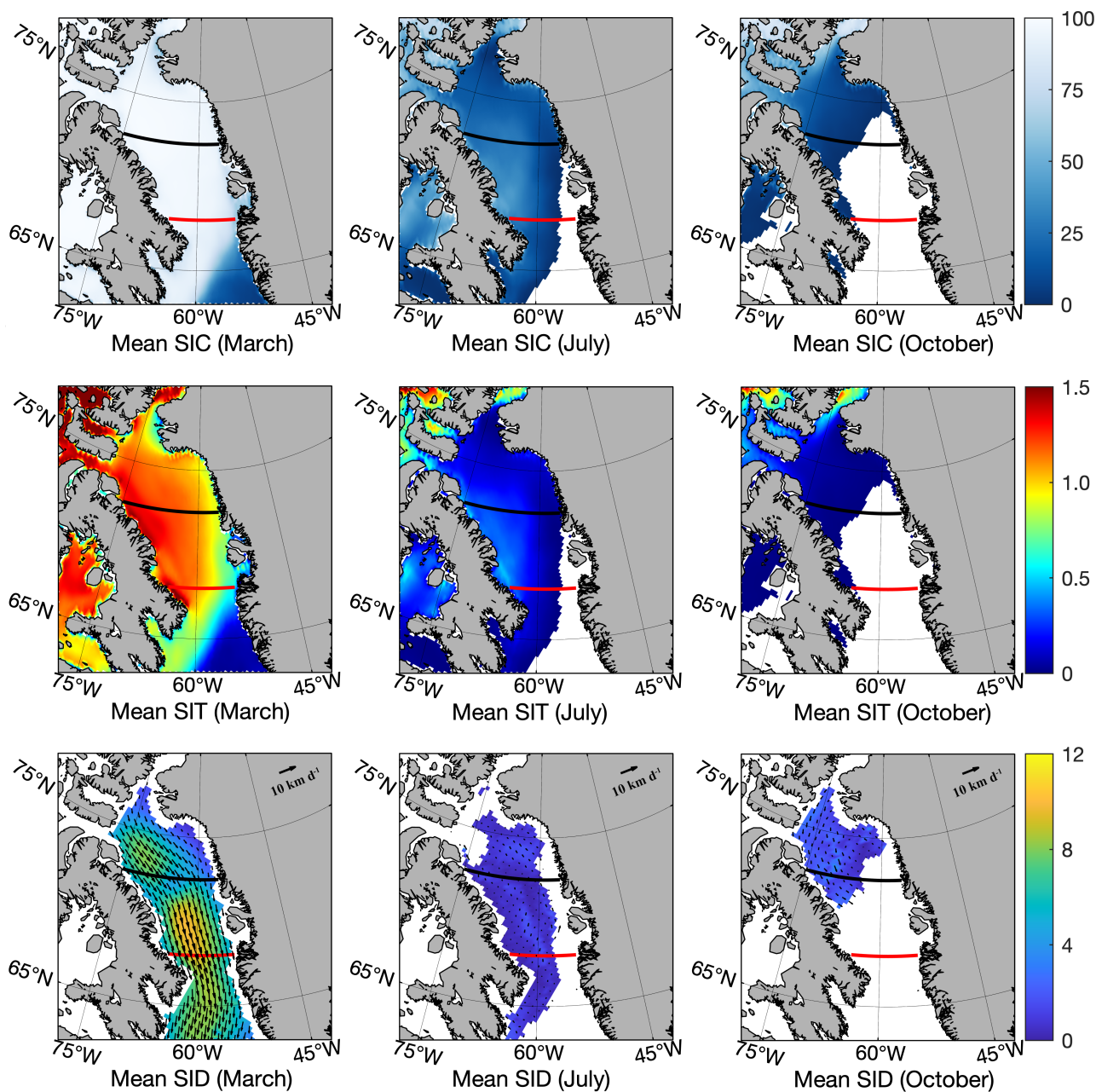
390

Figure 1. The ensemble mean sea ice concentration (top row: SIC, unit: %) and thickness (middle row: SIT, unit: m) from CMST, NAOSIM and PIOMAS for the long-term March, July, and October mean. The drift (bottom row: SID, unit: km d^{-1}) is from NSIDC. The black line shows the SIV inflow gate, and the red line denotes the SIV outflow gate in the Baffin Bay.
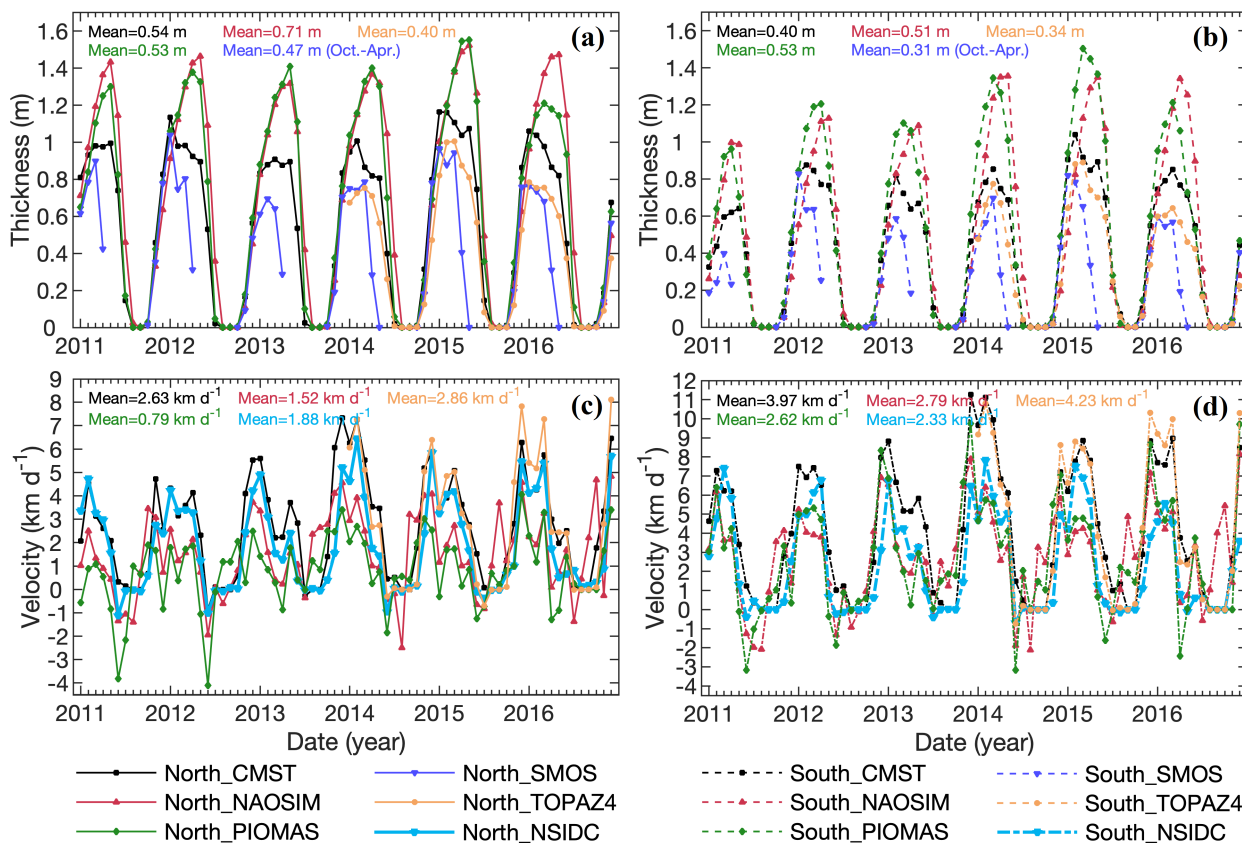
Figure 2. The monthly mean variations of sea ice thickness and southward velocity over the northern inflow gate and southern outflow gate (SIT: a and b, SID: c and d). The full lines in the left panel and dashed lines in the right panel represent sea ice inflow gate and outflow gate, respectively. The different colours denote different input sea ice data.

The Cryosphere
Discussions

Open Access
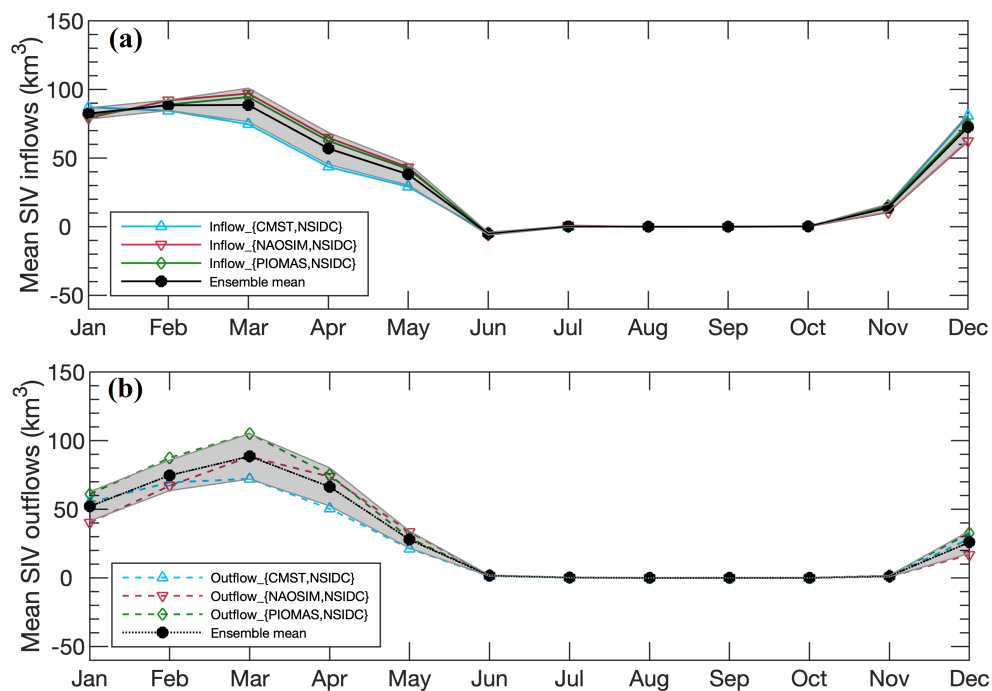
Figure 3. Averaged sea ice volume (SIV) (a) inflows through the north gate and (b) outflows through the south gate between 2011 and 2016. The cyan lines are the fluxes derived from CMST SIT and NSIDC SID, the red lines indicate estimations from NAOSIM SIT and NSIDC SID, the green lines denote the fluxes from PIOMAS SIT and NSIDC SID, and the black lines represent the ensemble mean fluxes from the three inflows and outflows, respectively. Shaded areas indicate the standard deviation derived from three different inflows and outflows, respectively.
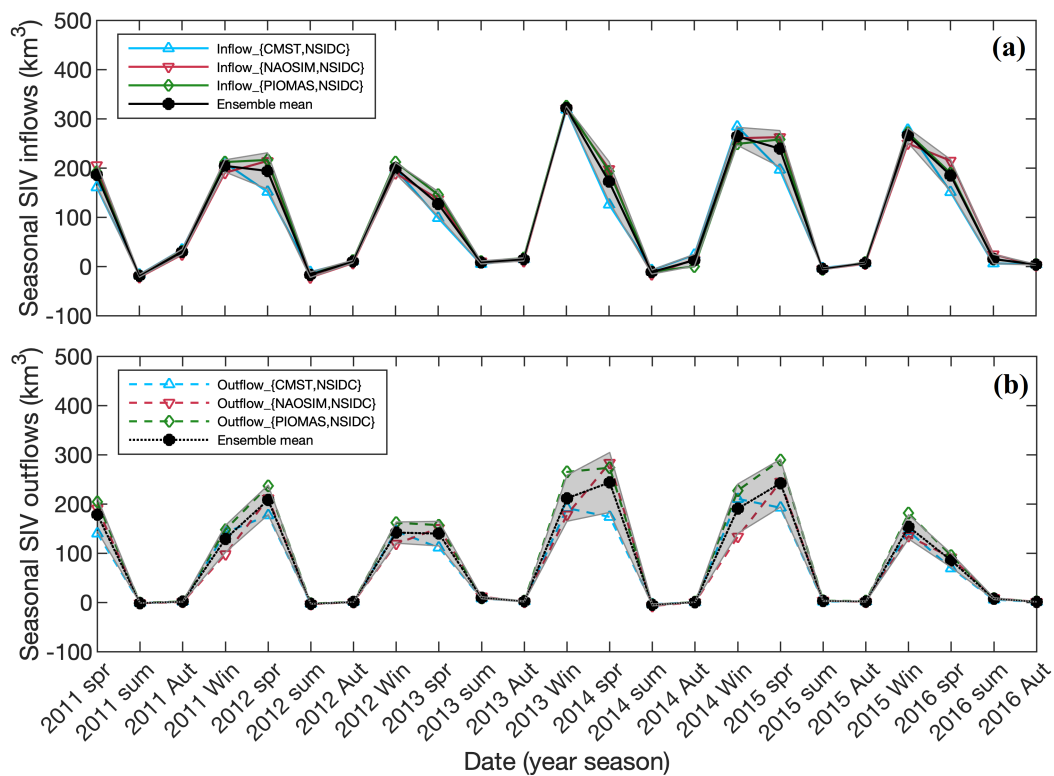
Figure 4. As Fig. 3 but for the long-term seasonal evolution of sea ice inflows and outflows.
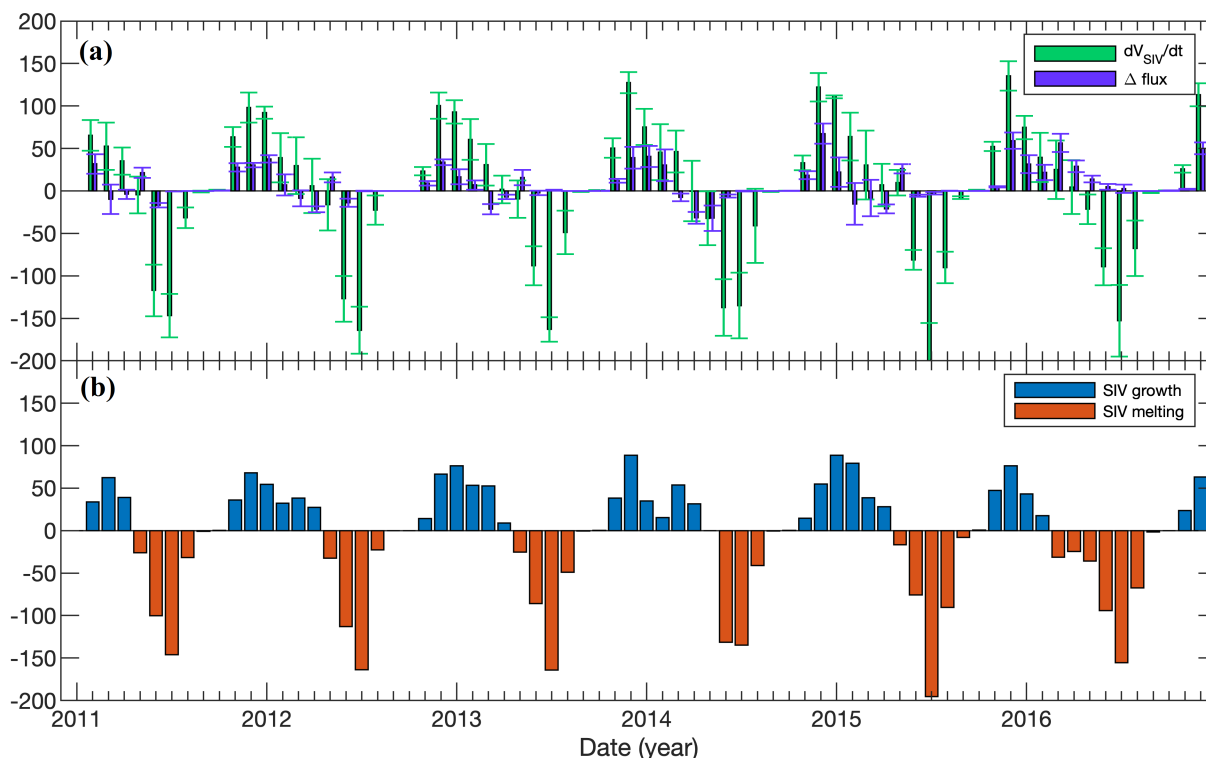
Figure 5. The ensemble mean sea ice volume changes from net ice flux and thermodynamics growth. (a) The ensemble mean SIV variability (dV_{SIV}/dt, green bar) in the defined Baffin Bay area and the net SIV flux (Δflux, purple bar) together with the ensemble spread (error bar). (b) The SIV variability derived from ice freezing (blue bar) and melting (orange bar) in the defined area.
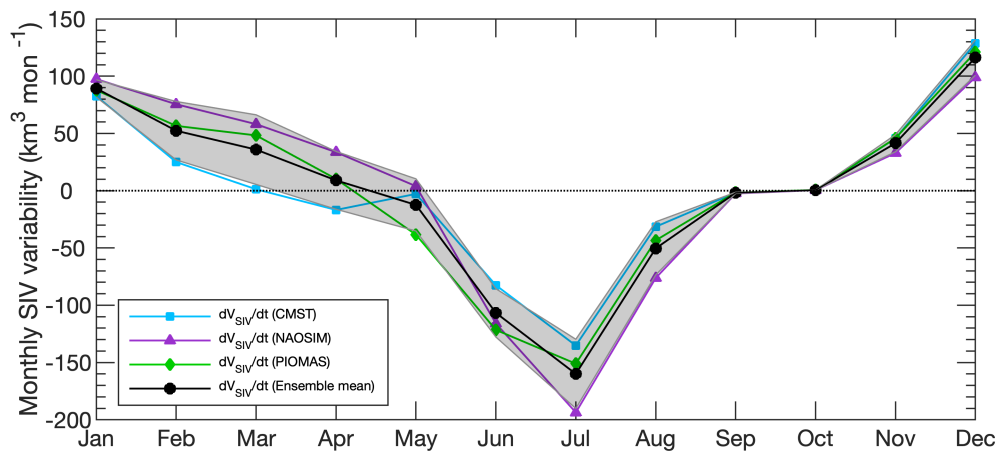
Figure 6. The sea ice volume variabilities from CMST (dV_{SIV}/dt (CMST), cyan line), NAOSIM (dV_{SIV}/dt (NAOSIM), purple line), PIOMAS (dV_{SIV}/dt (PIOMAS), green line) and the ensemble mean (dV_{SIV}/dt (Ensemble mean), black line) in the Baffin Bay area. The shading indicates the ensemble spread (one standard deviation).

Table 1. Monthly mean fresh water fluxes (km^3 month^{-1}) imported into the Labrador Sea that derived from the sea ice volume inflows.

	Jan	Feb	Mar	Apr	May	Jun	Jul	Aug	Sep	Oct	Nov	Dec
CMST_NSIDC	44	56	58	40	17	1	0	0	0	0	1	23
NAOSIM_NSIDC	32	54	71	60	27	1	0	0	0	0	1	13
PIOMAS_NSIDC	49	70	84	60	23	1	0	0	0	0	1	26
Ensemble mean	42	60	71	53	22	1	0	0	0	0	1	21